Available online at www.sciencedirect.com
SCIENCE DIRECT®
Ocean Modelling 10 (2005) 83–94
Ocean Modelling
www.elsevier.com/locate/ocemod

On some spurious mode issues in shallow-water models using a linear algebra approach

D.Y. Le Roux [a,*], A. Sène [b], V. Rostand [a], E. Hanert [c]

[a] *Département de Mathématiques et de Statistique, Université Laval, Québec, QC, Canada G1K 7P4*
[b] *Département de Mathématiques Appliquées, Université Gaston Berger, UFR SAT, BP 234, Saint Louis, Senegal*
[c] *Institut d'Astronomie et de Géophysique G. Lemaître, Université Catholique de Louvain, 2 Chemin du Cyclotron, B-1348 Louvain-la-Neuve, Belgium*

Received 10 December 2003; received in revised form 5 April 2004; accepted 1 July 2004
Available online 2 November 2004

Abstract

Numerical methods that are usually employed in ocean modelling are typically finite-difference, finite and spectral-element techniques. For most of these methods the coupling between the momentum and continuity equations is a delicate problem and it usually leads to spurious solutions in the representation of inertia-gravity waves. The spurious modes have a wide range of characteristics and may take the form of pressure (surface-elevation), velocity and/or Coriolis modes. The modes usually cause aliasing and an accumulation of energy in the smallest-resolvable scale, leading to noisy solutions. The Fourier analysis has proven practical and beneficial to describe the spurious solutions of several classical schemes. However it is restricted to uniform meshes on which the variables are regularly distributed. In this paper, a linear algebra approach is proposed to study the existence and the behaviour of stationary spurious modes associated with zero frequency, for some popular finite-difference and finite-element grids. The present approach is performed on uniform meshes but it applies equally well to regular as well as unstructured meshes with irregular geometry for the finite-element schemes.

* Corresponding author. Tel.: +1 418 656 7348; fax: +1 418 656 2817.
E-mail address: dleroux@mat.ulaval.ca (D.Y. Le Roux).

1463-5003/$ - see front matter © 2004 Elsevier Ltd. All rights reserved.
doi:10.1016/j.ocemod.2004.07.008

Keywords: Ocean modelling; Shallow-water equations; Spurious computational modes; Finite-difference method; Finite-element method

1. Introduction

The shallow-water equations are of considerable importance for a variety of problems of coastal and environmental engineering, including oceanic, atmospheric and groundwater flows. Oceanic models typically employ gridpoint, finite and spectral-element techniques. However, most of these methods may lead to spurious solutions in the representation of inertia-gravity waves (Batteen and Han, 1981; Williams, 1981), when solving the shallow-water and Navier–Stokes equations.

Walters and Carey (1983) investigated the nature of spurious pressure modes by means of a one-dimensional Fourier analysis of the linearized shallow-water equations. They found that spurious solutions may arise from the coupling of the momentum and continuity equations when representing inertia-gravity waves. This problem is encountered in both finite-difference and finite-element formulations. Its severity depends upon the placement of velocity and surface-elevation (or pressure) variables on a mesh, and upon the choice of appropriate basis functions for finite-element discretizations.

The spurious modes usually take the form of surface-elevation, velocity and/or Coriolis modes. They are small-scale artifacts introduced by the spatial discretization scheme which do not propagate but are trapped within the model grid, and associated with zero frequency. If the spurious solutions are left undamped, they can cause an accumulation of energy in the smallest-resolvable scale, leading to noisy solutions.

For example, subject to the no-slip boundary condition the B-grid (Mesinger and Arakawa, 1976) exhibits surface-elevation modes and hence a checkerboard pattern of noise in both the gravity wave and inertial limits, while the C-grid (Mesinger and Arakawa, 1976) is prone to Coriolis modes in the inertial limit only, provided the grid resolution is low relative to the Rossby radius of deformation (Walters and Carey, 1984). The finite-element pairs P_1–P_1 and P_1–P_0 (Brezzi and Fortin, 1991) suffer from surface-elevation modes in a similar manner as for the A- and B-finite-difference grids (Walters and Carey, 1983; Le Roux et al., 1998). The B- and C-grids and the P_1–P_1 and P_1–P_0 pairs are described later in Section 3.

Attention has been focused almost exclusively on the spurious surface-elevation modes since these were argued to be the most troublesome (Walters and Carey, 1983). A number of arguments have been advanced to explain their origin and to provide a basis for selecting grids that perform well. This has resulted in several strategies using the following methods: mixed-order finite-element interpolation (Walters and Cheng, 1980; Walters, 1983), equal-order elements with variables carried at sets of points staggered in space (Williams, 1981; Hua and Thomasset, 1984), vorticity and divergence instead of velocity in the momentum equations (Staniforth and Mitchell, 1977) and wave-equation (Lynch and Gray, 1979) and Petrov–Galerkin (Hughes et al., 1986) formulations.

The Fourier analysis has proven practical and beneficial to describe the spurious solutions of several classical finite-difference and finite-element schemes (Walters and Carey, 1983). However, it is restricted to uniform meshes on which the variables are regularly distributed.

Triangular finite-elements are attractive for ocean modelling due to their inherent flexibility for representing irregular boundaries and for local mesh refinement. However, the finite-element method has not been widely used in ocean modelling to date. This is because the ocean modelling community has been using finite-difference techniques for a long time and did not invested significant efforts to develop finite-element approaches.

For most of existing finite-element schemes the occurrence of spurious solutions is implicitly linked to an imbalance in the number of degrees of freedom between the discrete surface-elevation and the two components of the discrete velocity vector (Le Roux et al., 1998). It is then crucial to describe the behaviour of the spurious modes and their impact on the quality of the numerical solution, and possibly try to cure them. On structured meshes, macro element techniques (Brezzi and Fortin, 1991) may permit to "eliminate" the spurious modes. On unstructured meshes this is usually more difficult, and appropriate filtering techniques or the use of artificial dissipation are usually employed.

This paper is a first step towards the understanding of the behaviour of spurious solutions that may arise on unstructured grids. In order to do so, a linear algebra approach is proposed to study the existence and the behaviour of stationary spurious modes associated with zero frequency, for some popular finite-difference and finite-element grids. The present approach is performed on uniform meshes but it applies equally well to regular as well as unstructured meshes with irregular geometry for the finite-element schemes. The two-dimensional linearized form of the shallow-water equations are used in their inviscid and viscous forms, with appropriate boundary conditions, including the Coriolis terms.

The paper is organized as follows. The model equations are presented in Section 2. The discrete spurious modes are then examined in Section 3 for several popular finite-difference and finite-element schemes, in both inviscid and viscous cases. In Section 4, some concluding remarks complete the study.

2. The shallow-water model

2.1. Governing equations

Let Ω be the model domain with boundary Γ. The inviscid linear shallow-water equations are expressed in Cartesian coordinates (LeBlond and Mysak, 1978) as

$$\mathbf{u}_t + f\mathbf{k} \times \mathbf{u} + g\nabla\eta = 0, \tag{1}$$

$$\eta_t + H\nabla \cdot \mathbf{u} = 0, \tag{2}$$

where $\mathbf{u} = (u, v)$ is the horizontal velocity field, η is the surface-elevation with respect to the reference level $z = 0$, f and g are the Coriolis parameter and gravitational acceleration, respectively; $\mathbf{k}$ is a unit vector in the vertical and the mean depth H is assumed constant. Note that η plays the role that pressure plays in the Navier–Stokes equations. For a contained flow, Eqs. (1) and (2) are solved subject to the no-normal flow boundary condition

$$\mathbf{u} \cdot \mathbf{n} = 0 \quad \text{on } \Gamma, \tag{3}$$

where $\mathbf{n}$ is the outward pointing normal at the boundary.

2.2. The free modes

In the continuum case the free modes of (1) and (2) are examined by perturbing about the basic state $u = v = \eta = 0$. We seek solutions of (1) and (2) of the form $(u, v, \eta) = (\tilde{u}, \tilde{v}, \tilde{\eta})e^{i(kx+ly+\omega t)}$, where k and l are the wave numbers in the x- and y-directions, respectively, and ω is the angular frequency. Substitution into (1) and (2) then leads to a square matrix system for the Fourier amplitudes $\tilde{u}$, $\tilde{v}$, $\tilde{\eta}$. For a non-trivial solution to exist, the determinant of the matrix must equal zero, and this constraint leads to the following dispersion relation for the frequency

$$\omega(\omega^2 - f^2 - gH(k^2 + l^2)) = 0. \tag{4}$$

The first solution $\omega = 0$ is the geostrophic mode and it would correspond to the slow Rossby mode on a β-plane, while the other two solutions $\omega = \pm (f^2 + gH(k^2 + l^2))^{1/2}$ correspond to the free-surface gravitational modes with rotational correction. Since ω is purely real, all modes are neutrally stable and neither amplify nor decay.

3. Examination of the spurious discrete modes

3.1. A Fourier approach

Walters and Carey (1983) examined the numerical dispersion relations of the shallow-water and the compressible Navier–Stokes equations using a Fourier approach. For a given spatial scheme, in which the velocity and surface-elevation variables are uniformly distributed on a regular mesh, a set of selected discretized equations is obtained. Solutions of the form $(u, v, \eta) = (\tilde{u}, \tilde{v}, \tilde{\eta})e^{i(kx+ly+\omega t)}$ are again sought. Substitution into the selected discretized equations leads to a square matrix system for the Fourier amplitudes $\tilde{u}$, $\tilde{v}$, $\tilde{\eta}$. For a non-trivial solution to exist, the determinant of the matrix must equal zero. This constraint leads to a dispersion relation for the frequency, from which the eigensolutions may then be obtained analytically using appropriate boundary data. In their study, where the Coriolis effects are not considered, Walters and Carey (1983) described two basic sets of spurious modes.

For the first set, the velocity field is zero and non-constant elevation/pressure functions lie in the null space of the discrete gradient operator. Solution uniqueness is then lost since any multiple of a spurious mode can be added to any solution of the discrete equations and still satisfy them. It was also noted that this family of spurious modes is common to discretizations of both the shallow-water and the (compressible or incompressible) Navier–Stokes equations. For solution uniqueness, the null space of the discrete gradient operator must only contain constant surface-elevation functions, reflecting the fact that surface elevation is only determined to within an arbitrary additive constant, determined by fixing the surface-elevation reference level.

The second set of possible modes are those for which the elevation is zero and the velocity field is in the null space of the discrete divergence operator. Having noted their possible existence, little else is said about them in Walters and Carey (1983). Attention is focused almost exclusively on the spurious elevation modes of zero velocity, since these are argued to be the most troublesome. The occurrence of such spurious elevation solutions has been observed in a variety of finite-difference

(Walters and Carey, 1984) and finite-element (Walters, 1983; Le Roux, 2001) approximations to the shallow-water equations.

The Fourier analysis is restricted to uniform meshes on which the variables are regularly distributed. As a first step towards the understanding of the behaviour of spurious solutions on unstructured meshes, a linear algebra approach is now investigated, including the Coriolis effects.

3.2. A linear algebra approach

The linear algebra approach described herein is based on the study of the discrete operators (e.g. gradient, divergence, Coriolis) obtained by discretizing (1) and (2) in time and space. The velocity and surface-elevation components of the spurious solutions, if they exist, are then searched in the null space of these discrete operators. As previously mentioned, such a study applies equally well to uniform as well as unstructured meshes with irregular geometry. As a first step, only uniform meshes will be considered in the following.

For a given time step $\Delta t = t^{n+1} - t^n$ we introduce a general time discretization scheme of the form

$$\frac{\mathbf{u}^{n+1} - \mathbf{u}^n}{\Delta t} + f\mathbf{k} \times (\gamma \mathbf{u}^{n+1} + [1-\gamma]\mathbf{u}^n) + g(\alpha \nabla \eta^{n+1} + [1-\alpha]\nabla \eta^n) = 0, \tag{5}$$

$$\frac{\eta^{n+1} - \eta^n}{\Delta t} + H(\alpha \nabla \cdot \mathbf{u}^{n+1} + [1-\alpha]\nabla \cdot \mathbf{u}^n) = 0 \tag{6}$$

with $0 \leqslant \alpha \leqslant 1$ and $0 \leqslant \gamma \leqslant 1$. Observe that $\alpha = \gamma = 0,1/2,1$ yield the respective forward Euler, Crank–Nicolson and backward Euler type schemes.

Eqs. (5) and (6) are then discretized in space and rewritten in matrix form as

$$\mathsf{A}\mathbf{X}^{n+1} = \mathsf{B}\mathbf{X}^n \tag{7}$$

with $\mathbf{X}^n = (\mathbf{u}_1^n, \ldots, \mathbf{u}_N^n, \eta_1^n, \ldots, \eta_M^n)$ at time t^n and

$$A = \begin{pmatrix} \mathsf{M}^{\mathbf{u}} + \gamma \mathsf{C} & \alpha \mathsf{G} \\ \alpha \mathsf{D} & \mathsf{M}^{\eta} \end{pmatrix} \quad \text{and} \quad B = \begin{pmatrix} \mathsf{M}^{\mathbf{u}} + (\gamma - 1)\mathsf{C} & (\alpha - 1)\mathsf{G} \\ (\alpha - 1)\mathsf{D} & \mathsf{M}^{\eta} \end{pmatrix},$$

where $\mathsf{M}^{\mathbf{u}}$, M^{η} are the velocity and surface-elevation mass matrices, respectively, and C, G, D are the Coriolis, gradient and divergence discrete operators, respectively.

The surface-elevation, velocity and Coriolis spurious modes are specific eigenmodes associated with zero frequency. Hence, those modes have a zero phase speed, they do not propagate but are trapped within the model grid. We thus search for stationary eigenvectors $\mathbf{X} = (u_1, \ldots, \mathbf{u}_N, \eta_1, \ldots, \eta_M)$, such that $\mathbf{X}^{n+1} = \mathbf{X}^n$, associated with the generalized eigenvalue problem

$$\mathsf{A}\mathbf{X} = \lambda \mathsf{B}\mathbf{X}, \tag{8}$$

where $\lambda = 1$. Eq. (8) then leads to

$$\mathsf{A}\mathbf{X} = \mathsf{B}\mathbf{X}, \quad \text{i.e.} \quad (\mathsf{A}–\mathsf{B})\mathbf{X} = \mathbf{0}, \tag{9}$$

or, equivalently

$$\begin{pmatrix} \mathsf{C}_{N,N} & \mathsf{G}_{N,M} \\ \mathsf{D}_{M,N} & 0_{M,M} \end{pmatrix} \begin{pmatrix} \mathbf{u}_i \\ \eta_j \end{pmatrix} = \begin{pmatrix} 0 \\ 0 \end{pmatrix} \tag{10}$$

with $i = 1, \ldots, N$ and $j = 1, \ldots, M$, independently of the parameters α and γ and the mass matrices $\mathsf{M}^{\mathbf{u}}$ and M^{η}.

We also let $E = (\mathsf{C}\,\mathsf{D})^t$.

We now introduce the schemes that are used for the spatial discretization. Eight candidate finite-element pairs and finite-difference grids (shown in Fig. 1) for representing velocity and surface-elevation are described and evaluated in the remainder of this paper. In particular, their ability to approximate the shallow-water system in a spurious mode-free manner is investigated using structured meshes. The grids employed correspond to biased right isoceles triangles for the finite-element pairs and regular squares for the finite-difference grids.

The two candidate finite-difference grids are the classical B- and C-grids of Mesinger and Arakawa (1976). For both schemes the elevation field is carried at the center of the computational cells, and the elevation and velocity variables are staggered in space. For the B-grid the two components of the velocity field are located at the cell corners, while the normal velocities are carried at cell edge midpoints for the C-grid.

Conventional finite-element terminology is adopted to describe the six candidate triangular finite-element pairs of this study. The nomenclature P_m–P_n means that velocity components and surface elevation are, respectively, represented as piecewise-defined polynomials of degree m and n. Enhancements of this basic terminology are introduced as needed. Five finite-element velocity/surface-elevation pairs denoted P_1–P_1, P_1^{NC}–P_1, P_1 iso P_2–P_1, P_2–P_1 and MINI are first described. Common to all five is a piecewise-linear continuous representation of surface-elevation and they differ from one another in their representation of velocity.

The P_1–P_1 pair has velocity and surface-elevation nodes co-located at triangle vertices and the corresponding basis functions are piecewise-linear. The P_1^{NC}–P_1 pair (Hua and Thomasset, 1984; Le Roux, submitted for publication), has velocity nodes at triangle edge midpoints and linear

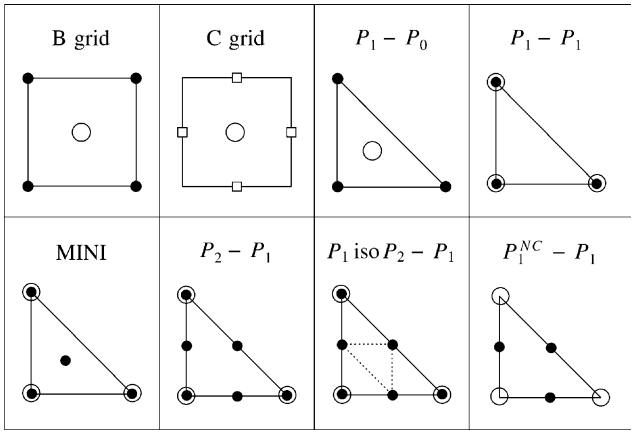

Fig. 1. Two finite-difference grids and six finite-element pairs are presented. The symbols (●) and (○) indicate velocity and surface-elevation nodes, respectively, while the symbol (□) indicates normal velocity nodes.

basis functions are used to approximate the two velocity components on the element's two-triangle support. Since this particular representation of velocity is only continuous across triangle boundaries at midpoint nodes, and discontinuous everywhere else around a triangle boundary, this element is termed non-conforming (NC) in the finite-element literature. The P_1 iso P_2–P_1 element pair (Bercovier and Pironneau, 1991) has piecewise linear basis functions for velocity on a refined triangulation obtained by dividing each triangle into four subtriangles using the midpoints of triangle sides. There are thus 6 velocity nodes over each unrefined triangle, the same as for a quadratic approximation of velocity, termed P_2. The designation P_1 in P_1 iso P_2 denotes linear velocity elements on subtriangles, whereas iso P_2 indicates that the nodal placement is that associated with quadratic elements on unrefined triangles. The P_2–P_1 pair (Hood and Taylor, 1974) has quadratic velocity basis functions while the MINI element has continuous piecewise-linear basis functions at the vertices and bubble functions at the barycenters for velocity (Arnold et al., 1984).

Finally, the last finite-element pair, the P_1–P_0 pair, has linear basis functions for velocity but discontinuous piecewise-constant basis functions for surface-elevation.

The eight finite-element and finite-difference schemes are now used to compute the dimension of the null space of the following matrices: G, D, C, A–B for $f = 0$ and $f \neq 0$, and E. The calculations are carried out using the numerical linear algebra routines of MATLAB and they are performed on a uniform 15×15 Cartesian mesh made up of 196 quadrilaterals or 392 biased right isoceles triangles. The no-normal flow boundary condition (3) is used and the results are summarized in Table 1. It should be noted that the numerical values used for the parameters ($f = 10^{-4}\,\mathrm{s}^{-1}$, $g = 9.81\,\mathrm{ms}^{-2}$, $H = 100\,\mathrm{m}$, $\Delta x = \Delta y = 20\,\mathrm{km}$), have no impact on the results.

3.2.1. Surface-elevation modes

Spurious surface-elevation modes correspond to the elevation part of the eigensolutions in (10) having zero velocity components. Hence, they are non-constant eigenvectors lying in the null space of the discrete gradient operator. Solution uniqueness is then lost since any multiple of a spurious mode can be added to any solution of the discrete equations and still satisfy them.

Table 1
Dimension of the null space of the matrices: G, D, C, A–B for $f = 0$ and $f \neq 0$, and E on a uniform 15×15 Cartesian mesh made up of 196 quadrilaterals. The inviscid case is considered with $\mathbf{u}\cdot\mathbf{n} = 0$ on Γ. The first column refers to the finite-difference grid or the finite-element pair type, while columns 2 and 3 indicate the number of velocity (N) and elevation (M) unknowns, respectively

Mesh 15×15	N	M	G	D	C	A–B $f = 0$	A–B $f \neq 0$	E
P_1–P_0	390	392	15	13	0	28	28	0
P_1–P_1	390	225	4	169	0	173	127	0
C-grid	364	196	1	169	26	170	170	1
B-grid	390	196	1	195	52	196	146	1
P_1^{NC}–P_1	1176	225	1	952	56	953	171	1
MINI	1174	225	1	950	0	951	125	0
P_2–P_1	1566	225	1	1342	0	1343	87	0
P_1 iso P_2–P_1	1566	225	1	1342	0	1343	87	0

Among the schemes examined in Table 1, only the finite-element pairs P_1–P_0 and P_1–P_1 exhibit elevation modes since the null space of their discrete gradient operator is more than one-dimensional. The dimension of the null space increases with increasing grid resolution for the P_1–P_0 pair while this is not observed for the P_1–P_1 pair. This is due to the fact that there are twice as many discrete continuity equations for the P_1–P_0 pair than discrete momentum equations to satisfy them. For the other finite-element pairs and finite-difference grids the null space of the discrete gradient operator is one-dimensional. The corresponding eigenvector is the hydrostatic mode, which can be simply considered as a constant of integration associated with the solution of the governing equations.

3.2.2. Coriolis modes

Coriolis modes may be defined as the velocity part of the eigensolutions in (10) having zero (or constant) surface-elevation components. They are thus non-constant eigenvectors lying in the intersection of the null spaces of the discrete Coriolis and divergence operators, i.e. the null space of E, and they correspond to the inertial limit case.

In Table 1, it is observed that only the finite-difference B- and C-grids and the finite-element pair P_1^{NC}–P_1 may generate spurious Coriolis modes. Indeed, the null space of the discrete Coriolis operator is zero-dimensional for the other pairs. The last column in Table 1 gives the dimension of the null space of E. It thus appears that the B- and C-grids and the P_1^{NC}–P_1 pair only exibit one Coriolis mode each, and this result is independent of the grid resolution. However, the Coriolis spurious mode associated with the C-grid is quite different from those of the B-grid and the P_1^{NC}–P_1 pair.

Indeed, because the mass matrices for the P_1^{NC}–P_1 pair and the B-grid are diagonal, the strong enforcement of the no-normal flow boundary condition introduces several lines of zero entries in the Coriolis matrix, and those exactly coincide with the number of boundary nodes. Hence, the null space of the discrete Coriolis operator corresponds to the number of boundary nodes for the B-grid and the P_1^{NC}–P_1 pair. As a result, those schemes exhibit a Coriolis mode having non-zero tangential velocities at the boundary nodes of the domain and zero velocities elsewhere. The spurious mode takes the form of a curl vector propagating around the boundary. Some elementary calculations show that this type of Coriolis mode is easy to compute and filter, even for the P_1^{NC}–P_1 pair on unstructured meshes with irregular boundaries.

The Coriolis mode associated with the C-grid is mainly due to the spatial averaging of the Coriolis terms on the grid and it behaves quite differently. Indeed, this mode takes the form of a set of identical cells located around some interior points obtained by joining the horizontal and vertical lines defining the grid. Let (i, j) the position of such a point. The cells are then defined by $v(i+\frac{1}{2}, j) = 1$, $u(i, j+\frac{1}{2}) = -1$, $v(i-\frac{1}{2}, j) = -1$ and $u(i, j-\frac{1}{2}) = 1$. To circumvent the Coriolis modes of the C-grid in the inertial limit, the C–D grid has been introduced (Adcroft et al., 1999). It consists of augmenting the C-grid variables with D-grid velocity variables.

3.2.3. Velocity modes

The last kind of stationary spurious modes that are now examined are termed velocity modes. To date, those modes do not seem to have been thoroughly examined. Velocity modes may be defined as the velocity part of the eigensolutions in (10) having non-constant surface-elevation components.

When $f = 0$, then $\mathsf{C} = 0$ in (10), and the dimension of the null space of (A–B) is simply the dimension of the null space of G plus the dimension of the null space of D, which is easily observed in Table 1. In this case the eigensolutions have constant surface-elevation components if the scheme is free of elevation modes and non-constant surface-elevation components otherwise. The velocity part of the eigensolutions lies in the null space of the discrete divergence operator and may thus contain curl vectors (which are highly desirable) and true spurious solutions as well.

When $f \neq 0$, Table 1 shows that the dimension of the null space of (A–B) is considerably reduced, except for the C-grid and the P_1–P_0 pair. Some long and tedious algebra shows that the dimensions of the discrete divergence and curl operator exactly coincide for the C-grid. Hence, each velocity vector lying in the null space of the divergence operator may be written in the form of a curl vector of some scalar function, at the discrete level. Note this property comes in part from the fact that after applying the no-normal flow boundary condition there are no remaining velocity unknowns on the boundary. The image of the curl vector by the Coriolis operator behaves like a gradient, and because the null space of the gradient operator is one-dimensional this explain why the Coriolis term has no effect upon the null space of (A–B) for the C-grid.

For the B-grid and the other finite-element pairs of Table 1, the null space of (A–B), even reduced by the influence of the Coriolis operator, may still contains spurious modes among the desirable curl vector solutions. In order to estimate the number of spurious modes for the schemes of Table 1, the dimension of the discrete curl operator has to be determined. The main difficulty is to take into account the influence of the boundary at the discrete level. This will be the object of a further study.

3.3. The viscous case

We now consider the viscous linear shallow-water equations in Cartesian coordinates

$$\mathbf{u}_t + f\mathbf{k} \times \mathbf{u} + g\nabla\eta - v\Delta\mathbf{u} = 0, \tag{11}$$

$$\eta_t + H\nabla \cdot \mathbf{u} = 0, \tag{12}$$

subject to the no-slip boundary condition $\mathbf{u} = 0$ on Γ, where v is a positive diffusivity parameter. As for the inviscid case, the system (11) and (12) is then discretized in time and space and rewritten on the matrix form

$$\begin{pmatrix} \mathsf{L}_{N,N} + \mathsf{C}_{N,N} & \mathsf{G}_{N,M} \\ \mathsf{D}_{M,N} & 0_{M,M} \end{pmatrix} \begin{pmatrix} \mathbf{u}_i \\ \eta_j \end{pmatrix} = \begin{pmatrix} 0 \\ 0 \end{pmatrix} \tag{13}$$

with $i = 1, \ldots, N$ and $j = 1, \ldots M$, and L represents the discrete Laplacian matrix.

We also let $F = (\mathsf{L}\,\mathsf{D})^t$.

The eight finite-element and finite-difference schemes proposed earlier are used to compute the null space of the following matrices: G, D, C, A–B for $f = 0$ and $f \neq 0$, and F. The grid and parameters are the same as those used earlier to compute the results of Table 1, except that the no-slip boundary condition is now imposed with $v = 500\,\mathrm{m^2\,s^{-1}}$. The results are summarized in Table 2.

As for the inviscid case the finite-element pairs P_1–P_0 and P_1–P_1 exhibit elevation modes since the null space of their discrete gradient operator is again more than one-dimensional. But

Table 2
Dimension of the null space of the matrices: G, D, C, A–B for $f = 0$ and $f \neq 0$, and F on a uniform 15×15 Cartesian mesh made up of 196 quadrilaterals. The viscous case is considered with $\mathbf{u} = 0$ on Γ. As for Table 1, columns 2 and 3 indicate the number of velocity (N) and elevation (M) unknowns, respectively

Mesh 15×15	N	M	G	D	C	A–B $f = 0$	A–B $f \neq 0$	F
B-grid	338	196	2	144	0	2	2	0
P_1–P_0	338	392	54	0	0	54	54	0
P_1–P_1	338	225	8	125	0	8	8	0
C-grid	364	196	1	169	26	1	1	0
MINI	1122	225	1	898	0	1	1	0
P_1^{NC}–P_1	1120	225	1	896	0	1	1	0
P_2–P_1	1458	225	1	1234	0	1	1	0
P_1 iso P_2–P_1	1458	225	1	1234	0	1	1	0

contrary to the inviscid case the B-grid has now 2 spurious surface-elevation modes since those are no longer linked by the no-normal flow boundary condition. Note that only the null space of P_1–P_0 increases with increasing grid resolution. For the other finite-element pairs and finite-difference grids the null space of the discrete gradient operator is one-dimensional and it just contains the hydrostatic mode.

In Table 2, it is observed that the B-grid and the P_1^{NC}–P_1 pair do not exhibit Coriolis modes contrary to the inviscid case. This is due to the no-slip boundary condition which prevents the appearance of lines of zero entries in the Coriolis matrix, since there are no longer velocity unknowns lying on the boundary. However, the Coriolis mode associated with the C-grid, and due to the spatial averaging of the Coriolis terms on the grid, is still present and it remains unchanged in the viscous case. Note the dimension of the null space of E is still one for the C-grid.

Finally, the dimension of the null space of (A–B) in Table 2 remains the same in the case $f = 0$ and $f \neq 0$, which indicates that the Coriolis terms have no effect upon the results. Further, the null space of (A–B) exactly coincides with the null space of the discrete gradient operator. Consequently, the null space of (A–B) just contains the hydrostatic mode for the *MINI*, P_1^{NC}–P_1, P_2–P_1 and P_1 iso P_2–P_1 pairs. For each of those pairs, the multiple zero eigenvalue of (A–B) present in the inviscid case has been split into a number of non-zero eigenvalues under the influence of the discrete Laplacian operator. However, the numerical impact of the viscosity on the velocity modes, when they exist, is still unclear and this has not been yet precisely determined. Note the dimension of the null space of F is zero for all the finite-difference grids and finite-element pairs examined here.

4. Conclusion

Most of the numerical methods that are used in ocean modelling poorly approximate the representation of inertia-gravity waves and usually lead to spurious solutions. The spurious modes may take the form of surface-elevation, velocity and/or Coriolis modes, and have dramatic effects upon the existence and the quality of the numerical solution. The occurrence of spurious modes is a manifestation of loss of convergence.

In this paper, a linear algebra approach is proposed to study the behaviour of spurious solutions that may arise from the linearized form of the shallow-water equations. The existence and the behaviour of stationary spurious modes associated with zero frequency are addressed for some popular finite-difference and finite-element grids in both the inviscid and viscous cases.

Spurious velocity modes do not seem to have been thoroughly examined in the past. In order to better identify them and describe their behaviour more accurately, we have suggested to determine the null space of the discrete curl operator for a given numerical scheme. Further, there also exists non-stationary spurious solutions, e.g. inertial modes, that have not been examined in the present paper. All these issues will be the object of a further study.

Acknowledgments

This work is supported by grants to D.Y.L. from the Natural Sciences and Engineering Research Council (NSERC), and to D.Y.L. and V.R. from FQRNT (Fonds Québécois de la Recherche sur la Nature et les Technologies). E.H. is research fellow with the Belgian National Fund for Scientific Research (FNRS).

References

Adcroft, A.J., Hill, C.N., Marshall, J.C., 1999. A new treatment of the Coriolis terms in C-grid models at both high and low resolutions. Mon. Weather Rev. 127, 1928–1936.

Arnold, D.N., Brezzi, F., Fortin, M., 1984. A stable finite element for the Stokes equations. Calcolo 21, 337–344.

Batteen, M.L., Han, Y.J., 1981. On the computational noise of finite-difference schemes used in ocean models. Tellus 33, 387–396.

Bercovier, M., Pironneau, O., 1979. Error estimates for the finite element method solution of the Stokes Problem in the primitive variables. Numer. Math. 33, 211–224.

Brezzi, F., Fortin, M., 1991. Mixed and Hybrid Finite Element MethodsSpringer Series in Computational Mathematics, vol. 15. Springer-Verlag, Berlin.

Hood, P., Taylor, C., 1974. Navier–Stokes equations using mixed interpolation. In: Oden, J.T. (Ed.), Finite Elements in Flow Problems. The University of Alabama in Huntsville (UAH) Press, Huntsville, AL, USA, pp. 121–132.

Hua, B.L., Thomasset, F., 1984. A noise-free finite-element scheme for the two-layer shallow-water equations. Tellus 36A, 157–165.

Hughes, T.J.R., Franca, L.P., Balestra, M., 1986. A new finite element formulation for computational fluid dynamics: V. Circumventing the Babuska–Brezzi condition: a stable Petrov–Galerkin formulation of the Stokes problem accommodating equal-order interpolations. Comput. Meth. Appl. Mech. Eng. 59, 85–99.

LeBlond, P.H., Mysak, L.A., 1978. Waves in the Ocean. Elsevier, Amsterdam.

Le Roux, D.Y., 2001. A new triangular finite element with optimum constraint ratio for compressible fluids. SIAM J. Sci. Comput. 23, 66–80.

Le Roux, D.Y., 2003. Dispersion relation analysis of the $P_1^{NC} - P_1$ finite-element pair in shallow-water ocean models. SIAM J. Sci. Comput., submitted for publication.

Le Roux, D.Y., Staniforth, A., Lin, C.A., 1998. Finite elements for shallow-water equation ocean models. Mon. Weather Rev. 126, 1931–1951.

Lynch, D.R., Gray, W.G., 1979. A wave-equation model for finite-element tidal computations. Comput. Fluids 7, 207–228.

Mesinger, F., Arakawa, A., 1976. Numerical Methods used in Atmospheric Models. GARP Publications Series No. 17. WMO-ICSU.

Staniforth, A., Mitchell, H.L., 1977. A semi-implicit finite-element barotropic model. Mon. Weather Rev. 105, 154–169.
Walters, R.A., 1983. Numerically induced oscillations in finite-element approximations to the shallow-water equations. Int. J. Numer. Meth. Fluids 3, 591–604.
Walters, R.A., Carey, G.F., 1983. Analysis of spurious oscillation modes for the shallow-water and Navier–Stokes equations. Comput. Fluids 11, 51–68.
Walters, R.A., Carey, G.F., 1984. Numerical noise in ocean and estuarine models. Adv. Water Resour. 7, 15–20.
Walters, R.A., Cheng, R.T., 1980. Accuracy of an estuarine hydrodynamic model using smooth elements. Water Resour. Res. 16, 187–195.
Williams, R.T., 1981. On the formulation of the finite-element prediction models. Mon. Weather Rev. 109, 463–466.